Modelling of the Neutral Gas and Plasma Transport in the Scrape- off Layer and Divertor of ST40-Tokamak

A. Nicolai, M. Gryaznevich

Tokamak Energy Ltd., 173 Brook Drive, Milton Park, Abingdon, OX14 4SD, UK

Abstract.. The description of the plasma transport in the SOL of the ST40-divertor accounts for parallel and perpendicular heat conduction, perpendicular particle diffusion, parallel convection, recycling of the neutral particles. To compute the density and ionization rate of the neutral gas in the divertor of ST40, the pseudo-collision technique was applied. The backscattering model accounts for a smooth transition between specular and diffuse reflection. The potential sheath in front of the plate enforces a zero total charge flux of the incoming electrons, the released secondary electrons and the incoming ions. The main results are:
The deposition of the ionized neutrals d_c has a strong maximum at the separatrix, the density n_c has the opposite behaviour since $n_c \sim d_c/n_e$. The maximum density is $n_{cmax}=2\ 10^{12}/cm^3$ and falls off rapidly in the parallel direction. The simulation of the plasma transport shows a radial $T_e(T_i)$-e-folding length of ~ 3 cm. The ion temperature has a minimum at the plate due to the cooling by the neutrals.

Introduction

In ST40 (design parameters: R/a=0.4/0.25m, Bt=3T, Ipl=2MA flat top duration up to 1 sec, NBI-power 2MW, NBI-energy E_b=25-55 keV, ECRH - power 1-2 MW/1/) a double null poloidal divertor configuration is under investigation. The divertor scrape off region is characterized by the competition between the transports parallel and perpendicular to the magnetic field lines cut by metal plates. In the case of axisymmetry this is accounted for by the fluid plasma models coupled with montecarlo neutrals /2/ and for pumplimiters in /3/. A consequence of the competition is the short e-folding length of the loading of the plate coming from the influx hydrogen and impurity ions which are accelerated in the potential sheath in front of the plate. This potential sheath is determined by the electron and ion temperature in the scrape off layer and the secondary electron emission at the plate. It enforces total zero charge flux to the plate. The sheath potential in general increases the energy of the incoming ions and therefore the sputter rate. Thus the reduction of the sheath potential by the secondary electron emission will be taken into account.

Sheath theory and boundary conditions

The boundary conditions at the divertor plate account for the sheath theory at the plate. There the electron flux is controlled by the voltage U between the plasma and the plate. Due to the requirement of zero electric flux we get $n_i\Lambda_i v_i + \langle Z \rangle n_v \Lambda_v v_v + j_s \Lambda_s = n_e \Lambda_e v_e$. n_i, n_v, n_e are the hydrogen, impurity and electron densities, $j_s = \sigma_e \Lambda_e n_e v_e + \sigma_i(\Lambda_i n_i v_i + \Lambda_v n_v v_v)$ is the secondary electron flux density. The Boltzmann factors $\Lambda_{e,i,v,s}$ are in the case of electrons and hydrogen ions given by $\Lambda_e = \theta(-U)\exp(eU/kT_e) + \theta(U)$ and $\Lambda_i = \theta(U)\exp(-eU/kT_i) + \theta(-U)$. By replacing the index ‘ i ’ by ‘ s ’ and ‘ v ' the Boltzmann

factor for the ions becomes that for the secondary electrons and the impurities if eU is replaced by $eU\langle Z\rangle$. $v_{i,e,v} = \sqrt{\frac{2kT_{i,e,v}}{m_{i,e,v}}}$ are the thermal velocities of ions, electrons and impurity ions. $\langle Z\rangle$ is the charge number averaged aver all ionization stages. θ is the Heaviside step function. In the examples given below only negative U occur. Then the sheath is electron repelling and ion accelerating.

The plasma boundary condition at the separatrix are $T_e = T_i = 100$ eV, $n_i = 10^{13}/cm^3$. The velocity boundary condition at the plate is $v_x = \alpha\Lambda_i v_i$. The temperature boundary condition account at the plate for the energy fluxes into the sheath /4/ which must be equal to the convective and conductive fluxes parallel to the field.

Sputtering and Backscattering

Results of the MC-codes MARLOWE and TRIM , simulating the collision events in the solid state lattice, may characterize the sputtering and backscattering events. At low energy, in the threshold region, the normalized sputter rate /5/ may be used. In the here assumed stationary state coronal equilibrium is used to compute the densities of the impurity ions (Fe)

As neutral particles atoms and molecules arrising from reflection and dissociation are considered. An ion or neutral particle impinging on the solid state lattice may be backscattered after some collision events. This can in general be described by a three-dimensional distribution $\omega_{E,\theta}(E',\theta',\varphi')$ depending on the energy E and polar angle θ of the incident particle and on the energy E′ and the polar and azimuthal angles θ′and φ′ of the backscattered particle. As in /3/ it is assumed here that ω can be written in a factorized form: $\omega_{E,\theta}(E',\theta',\varphi') = R_P(E,\theta)R_E(E,\theta,E')S_\theta(\theta',\varphi')$. The particle and energy backscattering coefficients, R_P and R_E , respectively, account for the results used in /3/.S is the angular distribution. For small $E' \le E_{\min}$ the particle is assumed to stick and then it emerges as molecule H_2 with one half of its original weight.

Plasma and neutral gas transport

The competition between the transport parallel and perpendicular to the magnetic field is described as in /4/ by the continuity equation, for the momentum and energy conservation for both, electrons and ions. Thus the plasma parameters depend on the radial coordinate and the field line parameter, r and x in Figs 1 – 10. Viscosity is included in the momentum equation, but neglected in the energy equations. The neutral plasma interaction is accounted for by the density gain due to recycling and the charge exchange losses. The neutral gas parameters, density, temperature and the deposition profile, are computed by the pseudo collision

technique /3/. Neutral-neutral collisions are neglected. The diffusion coefficient D and the perpendicular heat diffusivities $\chi_{e\perp}$ and $\chi_{i\perp}$are assumed to be constant and the parallel heat diffusivities are taken from classical theory. In the examples given below D=1.7 10^3 cm^2/sec and $\chi_{e\perp} = \chi_{i\perp} = 4\ 10^4$ cm^2/sec was chosen to account for a radial decay length of around 3 cm.

Results

Fig. 1 shows the radial and parallel dependence of the electron temperature T_e. since the field line length at the x - point becomes infinity, a mean field line length equal to one half of the connection length, l=πqR~750 cm, was used. The radial extension is d=3.5 cm and the e-folding length ~3 cm. At x=l the plate is located, at x=0 the midplane, at r=0 the separatrix. and at r=d a plane with vanishing particle and energy fluxes. Due to the large parallel heat diffusivity T_e is constant parallel to the field lines. In contrast the ion temperature T_i (Fig. 2) is due to recycling lower at the plate than in the bulk of the scrape off plasma. The density (Fig. 3) has a maximum in the vicinity of the plate due to recycling. The deposition profile H (Fig. 4) of the neutrals gas (NG) has the maximum at the separatrix because the plasma flux density is there the largest. The NG density n_c (Fig. 5) has the opposite behaviour because of n_c~H/n_e. The decay of n_e is stronger than that of H. The NG temperature follows closely the ion temperature (Fig. 6). By means of T_e, T_i and n_p the sheath potential and the current densities described in the 2^{nd} section can be computed. Fig. 7 shows the radial dependences of the current densities of the incoming electrons (red) and ions (blue) and of the secondary electrons (green). As plate materials Fe and Mo were compared. The secondary electron emission coefficient of Fe (folded with a maxwellian) has a flat maximum (1.3) at 400 eV. At the separatrix the current densities of secondary electrons and ions almost agree so that the electron current density is twice as large as the ions current density. In contrast, the analogous Fig. 8, with Beryllium as plate material, the ion current density is around ¾ of the electron current density. The sputter rate follows from the sheath potential and the sputter coefficient, which is much lower for Mo than for Fe. Therefore the sputtered fluxes at a Mo – plate (9.5 10^{17}/sec) and at a Fe plate (6.2 10^{19}/sec) differ accordingly. Fig. 9 shows the impurity density (Fe) summed over all ionization stages. In stationary state coronal equilibrium may be a reasonable approximation. Fig. 10 (left) shows the ionisation stages of Fe. The electron temperature profile is that of Fig. 1. In Fig.10 (right) we have T_{emax}=200 eV. The dominating ionisation state is Fe^7 followed by the lower ionisation states Fe^6, Fe^5 at the outside and the higher ionization states as Fe^8 and Fe^9 at the inside in the vicinity of the separatrix.

Summary and Conclusions The modelling shows that the secondary electron flux density for a Fe plate is as large as the ion flux density what entails a reduction of sheath potential and of

the sputter rate at the plate. The sputtered flux at a Mo – plate is much lower than that at a Fe plate because of the much lower Mo - sputter coefficient. Although Mo is more 'toxic' than Fe, it is the more favourable plate material.

The maximum neutral gas density is consistent with plasma flux density to the plate. The opposite behaviour of n_c and H is due to $H \sim n_c\, n_e$.

The modelling suffers from the fact that the core plasma is accounted for by simple pedestal boundary conditions. Therefore an integrated modelling of core and SOL is needed/4/.

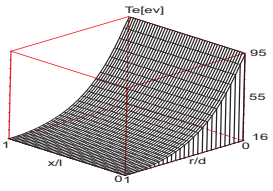

Fig.1 Electron temperature

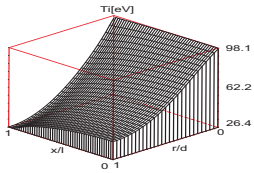

Fig.2 Ion temperature

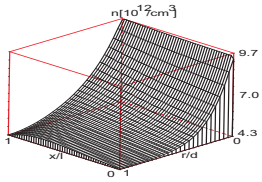

Fig.3 Proton density

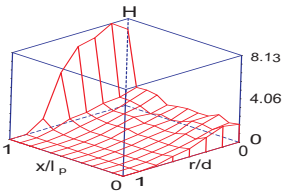

Fig.4 Deposition pofile of the NG

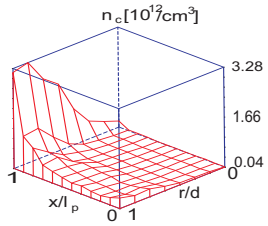

Fig. 5 Density of the NG

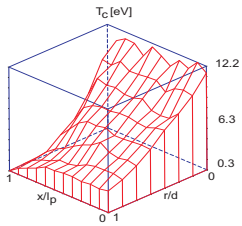

Fig.6 Temperature of the NG

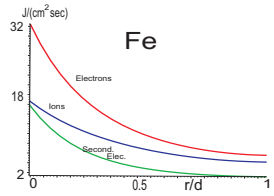

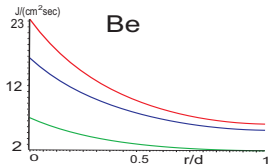

Fig. 8 Current densities at the plate(Fe left, Be right) .

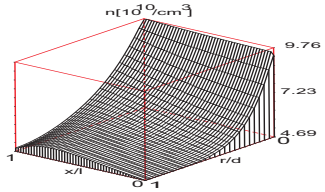

Fig.9 Impurity density build up by sputtering

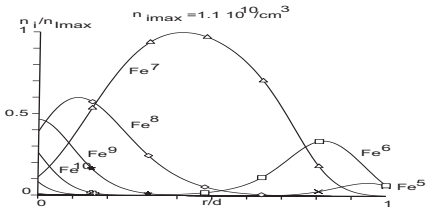

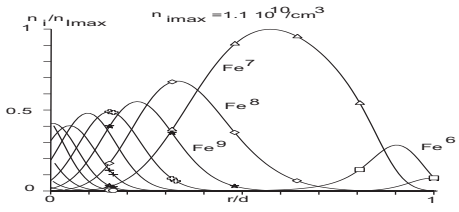

Fig.10 Distribution of the Fe ions Fe^5-Fe^{10} for T_{emax}=100eV(left) and T_{emax}=200 eV(right)

/1/ M. Gryaznevich O. Asunta and Tokamak Energy Ltd. Team. FED 123 (2017) 177-180
/2/ Bonnin X., et al. 2016 Plasma Fusion Res. 11 1403102
/3/ A.Nicolai et al., J. Comput. Phys.,106 (1993) 377-390
/4/ A.Nicolai et al., J. Nucl. Mater.145/147 (1987) 873-876
/5/ H.L. Bay, J. Roth, J. Bohdansky, J. Appl. Phys. 48 (1977) 4722